Argon Injection Optimization in Continuous Slab Casting

Tiebiao Shi and Brian G. Thomas

Continuous Casting Consortium
Dept. of Mechanical and Industrial Engineering
University of Illinois at Urbana-Champaign
1206 West Green St., Urbana, IL 61801

217-333-6919; 217-244-6534 (fax); bgthomas@uiuc.edu

Objectives:

1) Develop multiphase computational model to simulate the 3-D flow pattern of molten steel in the continuous casting mold with argon gas injection

2) Compare and evaluate differences between steel caster and scale water models

3) Estimate the flow pattern (single roll, double roll, etc.) obtained in the steel caster as a function of gas injection rate, liquid steel throughput (casting speed), mold width, and other important parameters (eg. argon bubble size)

4) Recommend practices related to argon gas injection optimization to improve steel product quality, especially as related to flow pattern.

Background

Argon is injected into continuous casting nozzles to perform several functions. Firstly, it is used to minimize nozzle clogging. It does this in several possible ways:

- A film of argon gas forms along on the nozzle wall to prevent inclusion contact with the wall [1, 2]. This mechanism is likely only at very high gas flow rates [3] and likely also causes flow disruptions in the mold [4]

- Argon bubbles attach to the inclusions and carry them away [5].

- Argon gas increases the turbulence, which dislodges delicate inclusion formations from the nozzle walls and breaks up detrimental concentration and surface tension gradients near the nozzle wall [6]. It is noted that this mechanism may sometimes be detrimental by increasing particle contact with the walls and enhancing deposition.

- Argon gas reduces air aspiration and reoxidation by increasing pressure inside the nozzle [2, 7-9]. Argon supplied through porous slits or into joints also helps by replacing air aspiration with argon aspiration.

- Argon retards chemical reactions between the steel and the refractory [5, 10].

In addition, argon greatly changes the flow pattern in the nozzle, and subsequently in the mold [11, 12]. Too much argon can cause the liquid and gas phases to separate, resulting in unstable flow and transient level fluctuation problems in the mold. [4]. Excessive argon also may cause quality problems from bubble entrapment. Too little argon requires the flow pattern to be controlled by nozzle geometry, submergence, and throughput alone, which may not be easy for wide slabs. Thus, it is very important to optimize the argon flow rate.

Past work has used scale water models to investigate the effects of argon injection. [12] However, the behavior of air / water systems may be different than that of argon / molten steel systems, owing to differences in properties which are difficult to account for. Thus, the present project was undertaken to apply 3D computational models to optimize argon injection for control of the mold flowpattern.

Model description

Computational models have been developed using the control-volume CFD code, CFX. The model solves the 3-D Navier Stokes equations using the K-ε turbulence model in half of the mold. Symmetry was assumed between the two mold halves, and the inlet condition is based on prior simulations of flow in the nozzle. The water model simulations simply fixed the inlet conditions to constants based on nozzle model results, while the steel flow simulations employed inlet conditions which varied at each node in the mold inlet plane (the nozzle port outlet) Multiphase flow was treated using the MUSIG model. This model treats the bubble distribution as a single phase separate from the liquid, but consisting of several different sizes. Each size range is transported separately throughout the domain and evolves according to both coalescence and breakup criteria.[13]

Flow patterns are classified according to the behavior of the surface velocity at the center between the SEN and narrow face. Flows directed towards the SEN are “double roll”, while flows directed towards the narrow face are “single roll”.

Model validation with water model flow

The current models have been validated with many detailed comparisons with PIV measurements in single phase flow.[3, 14-17] To validate them in multiphase flow, when the gas buoyancy effect is significant, two cases were chosen (See Tables IA and IB). Case A was chosen to match typical conditions in the caster where pencil pipe defects were sometimes encountered, but slivers were minimal (55 inches per minute; 13 SLPM gas flow; 73” wide). Case B was chosen to match a typical condition where slivers were sometimes present, but pencil pipe was not (35 inches per minute; 6.5 SLPM gas flow; 73” wide). Both cases were simulated using the 0.4-scale water model at LTV Steel, which involved changing the gas and liquid flow rates (according to Froude similarity criteria) to the values given in Tables IA and IB.

The most difficult aspect of setting up the computational modeling was determination of the bubble size distribution, which is known from previous work to be very important. (Large numbers of small bubbles provide more buoyancy to lift the flow pattern more than small numbers of large bubbles). Bubble size distributions were measured from still photographs of the operating water model, as described in Appendix I. The resulting size distributions for cases A and B are compared in Fig. 1, where it can be seen that case A had smaller, more uniformly-sized bubbles.

The calculated flow pattern results are compared with the water model measurements, both as visualized with photographs and using Particle Image Velocimetry. During the water modeling, it was discovered that significant variations in water flow were encountered due to random fluctuations in the liquid level. For Case A, the nominal 55 ipm actually varried from 54.00 – 70.01 ipm. For Case B, the nominal 35 ipm ranges from 34.86 ipm to 40.24 ipm. Thus, results were obtained for two extreme flow rates each for cases A and B and are presented in Figs. 2 and 3.

Fig. 2 shows results for steady casting, where the flow rate is constant. In Case A, the main jet is seen to impinge on the narrow face and move mainly downward. There is also a significant jet moving directly upward from the nozzle, which contains a high gas fraction. Competition between these two jets results in very slow velocities near the corner. This complex flow pattern should be classified as “transition flow”, as a sensor located midway between the SEN and narrow face might detect flow in either direction, changing with time. In Case B, on the otherhand, shows a consistent “single roll” flow pattern, where the jet immediately lifts to the top surface and flows across and down the narrow face.

Fig. 3 shows results during a flow transient when the flow rate was temporarily higher in order to raise the level back up. Fig. 3A shows that the temporary increase in velocity causes the liquid jet to penetrate deeper into the caster, which is most noticible by comparing the deep bubble penetration distance of Fig. 3A with the shallow distance of Fig. 2A. The overall flow pattern becomes generally "double roll". Thus, the case A flow pattern is unstable, as it can change drastically due to subtle changes in inlet conditions and bubble size. The Case B flow pattern, however, stays as a consistent single roll flow pattern in both cases.

The most significant finding here is that the simulation results agrees well with the water-model measurements for all four cases. The model is then applied to simulate expected behavior in the real steel caster.

Model prediction of steel caster flow

The steel caster is different from the water model in several important ways. Firstly, the bubble size distributions (shown in Fig. 4) are different in several ways, for several reasons explained in the Appendix. Specifically, the distributions change, showing more uniformity at the lower speed, while the mean bubble size is about the same, as seen by comparing Figs. 1 and 4. Secondly, the water model is smaller than the real caster (0.4 scale) and has lower liquid velocities. Although the input liquid velocity is based on Froude number similarity criteria, it has not been verified if this criterion produces a good match with the full-scale. Thirdly, the water and steel have different fluid properties (density and viscosity).

All of these differences were included in a CFX simulation of multiphase flow for the same cases A and B. Figs. 5 show the nozzle flow patterns, while Figs. 6-7 show the corresponding mold flow patterns front view (Figs. 6) and side view looking into the port (Figs. 7). The nozzle flow pattern reveals more horizontal flow due to stronger swirl for the higher speed case (A), which results in more flow towards and across the inner radius face of the mold (Fig. 6A). (The actual face which receives more impingement may change with time in addition to gate orientation and position).

Of greatest significance is the fact that both cases A and B are predicted to be generally double roll flow patterns. For Case A, flow along the surface near both faces is towards the SEN, while flow in the center is very slow and possibly reveresed. Below the SEN, flow along the inner face is towards the narrow face, while flow along the outer radius face is towards the SEN. This complexity illustrates how Case A is close to a transition flow situation, although it may still be classified as double roll.

Case B, on the other hand, exhibits more classic double-roll flow behavior. Flow from the nozzle has a less powerful swirl, so flow along the two faces is more symmetrical. The jet is generally shallower (due to the greater effect of gas buoyancy at the lower speed), but the flow pattern is consistently towards the SEN along the top surface. The jet first impinges on the narrow face. The bubble contours in case B all stay within the upper recirculation zone, indicating that bubble entrapment into the lower roll should be very rare. For Case A, on the other hand, the bubble contours extend further. Although still rare, Case A appears to have worse potential for bubble entrapment, as found in the plant.

The flow pattern measured by MFC sensors in the plant generally show a double-roll flow pattern for both cases A and B, which is consistent with these predictions. However, the plant measurements also show that case B experiences transition flow states, which be caused by transient structures breaking off from the jet, which is quite shallow and near to the surface. Especially if the nozzle submergence became shallower, or if the bubble size decreased or gas fraction increased, this case might exhibit detreimental transition behavior.

The most significant finding here is that the flow pattern in the steel caster is different from that in the water model and that the computation can match both! The differences are most striking for case B, which changes from a stable single-roll in the water model to an unstable double-roll flow pattern in the caster.

Parametric Study

Having a validated model, parametric studies can be performed to investigate the flow pattern expected in the real caster for different gas flow rates, casting speeds, and section sizes. First, to further investigate the stability of the flow pattern for case B, the gas content was increased from 6.3 to 13 SLPM (8.5% to 16.4%). The results are illustrated in Figs. 6C and 7C. This case exhibits a generally single-roll flow pattern, as flow is generally towards the narrow faces. This flow pattern appears to be only barely stable, however, as flow reverses in some regions near the faces. Considering cases B and C together, it appears that the transition from double to single roll occurs between the two extremes of 8.5% and 16.4%. Thus, an arbitrary critical limit of 12% gas entering the mold was assigned to this set of casting conditions. Gas fractions near this limit will have detrimental transition flow behavior. Gas fractions well above this limit should exhibit a single-roll flow pattern, while gas fractions well below this limit should exhibit a more stable double-roll flow pattern.

The critical gas fraction does not appear to be a strong function of throughput. This is shown in Fig. 8, which replots water model measurements [12]. Deviations from a constant critical gas fraction with throughput are most likely due to transitions in bubble size or size distribution, which needs further study. In this work, the 12% cutoff for a 73” mold is consistent with case A.

Corresponding critical gas fractions were estimated for other widths based on previous simulations by Creech.[17] Specifically, the critical gas fraction appears to be near about 20% gas for 52” wide. These limits are presented in Fig. 9 together with estimates of the transition range. Interpolation yields 15.8% for 63” wide, and 24.57% for 40” wide.

For easy practical interpretation in the plant, these critical values are converted to cold gas flow rates (SLPM) and presented in Fig. 10 as a function of liquid throughput and slab width. Each line on this graph indicates the estimated center of the critical transition region, which should be avoided for that width. It is recommended that argon gas injection should be limited to stay consistently and safely below these limits, in order to achieve a stable double-roll flow pattern that does not change with time.

Discussion

Flow Pattern Evaluation Criteria

Finding criteria to evaluate what flow pattern is best is very difficult. This is because the flow pattern is only an indirect indicator of quality issues, such as flux entrainment, level fluctuations, meniscus freezing, particle entrapment, and other problems. Work by Assar indicates that flow stability is more important than the actual flow pattern. Furthermore, flow stability is better with a double roll flow pattern than with a single roll pattern, and improves with lower gas flow, lower casting speed, and narrower widths. The present work is consistent with this finding and suggests furthermore that the complex transition flow patterns between single and double roll are the least stable (in this sense). Given this finding, it would appear that the argon flow rate should be kept below than the critical transition flow rate.

Model Simulation Results

Several model trends match those known from previous study and from water modeling, and are considered in the results and recommendations here:

1) Increasing argon gas fraction tends towards a single roll flow pattern, as the gas gives added lift to the jet. However, increased gas also decreases flow pattern stability, as the large bubbles will rise immediately and may cause detrimental transition flows.

2) Increasing throughput requires increased gas injection in order to produce the same jet buoyancy, and thereby the same flow pattern. Initial model results show that keeping a constant gas fraction generally is sufficient to achieve this, as a first estimate.

3) Increasing mold width (at constant throughput and gas flow rate) tends towards a single roll flow pattern due to two factors:
   - further travel required by the jet to reach the narrow face makes surface impingement more likely;
   - the gas fraction increases with the lower casting speed accompanying wider slabs

4) Increasing gas bubble size (by injecting into a region of lower liquid velocity, or decreasing the number of active sites where gas enters the nozzle, so that gas fraction stays constant) tends to make the flow pattern more double-roll, but may be less stable. Increasing the uniformity of the bubble size tends toward single roll (as the

gas lifting effect is more efficient), but makes the flow pattern more sensitive to changes in mean bubble size.

5) Increasing submergence depth (at constant throughput, gas flow rate and width) tends to encourage a double-roll flow pattern. For a given set of conditions, an optimum submergence depth exists that is deep enough to avoid unstable flow transitions, (to minimize surface turbulence) together with being shallow enough to allow sufficient top surface flow and heat transfer.

6) Argon gas optimization must consider factors beyond flow pattern, such as clogging prevention. Argon flow should be at least sufficient to maintain positive pressure inside the nozzle, by satifsying criteria stated elsewhere.[18] Furthermore, argon flow should be stable, so injection into regions of low-pressure or low liquid velocity should be avoided. In addition, argon flow should attach to bubbles so should ideally produce large numbers of small, uniform-sized inclusions. This requires optimization of the porous region and pressure drops inside the nozzle refractory.

<u>Error Sources</u>

It must be cautioned that this preliminary study is far from complete. Furthermore, it is extremely difficult to predict flow behavior due to argon injection without further experimental data for several reasons:

1) Not all of the injected argon goes down the nozzle into the mold. If there are leaks in the system between the flow measurement and injection points, some of the gas will be diverted.
2) The shape of any internal clogging interferes with the flow resistance and gas trajectories.
3) The size of the bubbles critically influences the flow pattern and the size is determined by the nature of the gas injection into the nozzle, the porous ceramic properties, the surface tension, the gas and liquid flow rates. [19]

Recommendations

1. Do not inject argon into the lowest pressure locations in the nozzle (eg. below the bottom plate of the slide gate, or just above the top plate). These low pressure regions will attract large gas flow rates locally, leading to large gas pockets (large bubble size from Bai's work) and potential flow instabilities.

2. Ramp the casting speed back up slowly after a ladle change (in order to minimize unstable transient flow, which is worst for quality).

3. Change submergence gradually (not suddenly) and try to arrange for the deeper submergence depths to occur the wider slabs and shallower for narrow slabs.

Remember that optimal argon injection depends on width, casting speed, and submergence depth.

4. Keep argon injection *below* the levels recommended for stable double roll flow (eg. as suggested in Fig. 10). (It is easier to keep the double roll flow pattern stable than it is for the single roll).

5. Vary argon injection rate with throughput, width, and submergence depth.

6. When casting speed drops severely (eg. 20 inches / min. or less during an abnormal severe slow-down, cut argon to zero or minimal flow rate such as 1 SLPM). Argon should be needed to prevent nozzle clogging due to air aspiration in these conditions; very little gas is needed to maintain a constant gas percentage; and bubble size might grow severely.

7. Further study is recommended using the mathematical models to quantify the conditions which lead to defects and then to fully quantify the flow patterns which lead to safe conditions through subsequent parametric studies. Further study is also needed of gas flow through the refractory relative to pressure drops in the nozzle in order to understand how the gas exits into the nozzle.

Acknowledgements

The authors would like to thank the National Science Foundation (NSF - Grant # DMI - 98-00274) and the Continuous Casting Consortium (CCC) at the University of Illinois at Urbana Champaign (UIUC) for their support of this research, the National Center for Supercomputing Applications (NCSA) at the UIUC for computing time, AEA technology for use of the CFX 4.2 program, and LTV Steel, especially Pierre Dauby and Mohammad Assar, for use of the water model and PIV system and access to PIV and MFC measurements.

References

1. T.R. Meadowcroft and R.J. Milbourne: "A New Process for Continuously Casting Aluminum Killed Steel", *Journal of Metals*, 1971, vol. June, pp. 11-17.

2. L.J. Heaslip, I.D. Sommerville, A. McLean, L. Swartz and W.G. Wilson: "Model Study of Fluid Flow and Pressure Distribution During SEN Injection - Potential for Reactive Metal Additions During Continuous Casting", *Iron and Steelmaker*, 1987, vol. 14 (8), pp. 49-64.

3.* H. Bai: *Argon Bubble Behavior in Slide-Gate Tundish Nozzles During Continuous Casting of Steel Slabs*, PhD Thesis, University of Illinois, 2000.

4. M. Burty, M. Larrecq, C. Pusse and Y. Zbaczyniak: "Experimental and Theoretical Analysis of Gas and Metal Flows in Submerged Entry Nozzles in Continuous Casting", in *PTD Conference Proceedings*, vol. 13, ISS, Warrendale, PA, Nashville, TN, 1995, pp. 287-92.

5. M.C. Tai, C.H. Chen and C.L. Chou: "Development and Benefits of Four-Port Submerged Nozzle for Bloom Continuous Casting", in *Continuous Casting 85 Proceedings*,,, Inst. of Metals, 1 Carlton Hourse, Terrace, London, UK, 1985, pp. 19.1-19.6.

6. A.W. Cramb and I. Jimbo: "Interfacial Considerations in Continuous Casting", *Iron & Steelmaker (ISS Transactions)*, 1990, vol. 11, pp. 67-79.

7. E.S. Szekeres: "Review of Strand Casting Factors Affecting Steel Product Cleanliness", *4th International Conference on Clean Steel*, Balatonszeplak, Hungary, 1992.

8. I. Sasaka, T. Harada, H. Shikano and I. Tanaka: "Improvement of Porous Plug and Bubbling Upper Nozzle for Continuous Casting", in *74th ISS Steelmaking Conference*, vol. 74, ISS, Warrendale, PA, 1991, pp. 349-56.

9.* H. Bai and B.G. Thomas: "Effect of Clogging, Argon Injection, and Casting Conditions on Flow Rate and Air Aspiration in Submerged Entry Nozzles Steel", in *83rd Steelmaking Conference Proceedings*, vol. 83, ISS, Warrendale, PA, Pittsburgh, PA, March 2-29, 2000, 2000, pp. 183-97.

10. F.L. Kemeny: "Tundish Nozzle Clogging - Measurement and Prevention", in *McLean Symposium Proceedings*,,, ISS, Warrendale, PA, 1998, pp. 103-10.

11. B.G. Thomas, X. Huang and R.C. Sussman: "Simulation of Argon Gas Flow Effects in a Continuous Slab Caster", *Metall. Trans. B*, 1994, vol. 25B (4), pp. 527-47.

12. M.B. Assar, P.H. Dauby and G.D. Lawson: "Opening the Black Box: PIV and MFC Measurements in a Continuous Caster Mold", in *Steelmaking Conference Proceedings*, vol. 83, ISS, Warrendale, PA, 2000, pp. 397-411.

13. CFX 4.2: AEA Technology, 1700 N. Highland Rd., Suite 400, Pittsburgh, PA 15241, Report, 1998.

14.* B.G. THOMAS, Quan YUAN, Sivaraj SIVARAMAKRISHNAN, Tiebiao SHI, S. P. VANKA and M.B. ASSAR: "Comparison of Four Methods to Evaluate Fluid Velocities in a Continuous Slab Casting Mold", *ISIJ International*, 2001, (Sept.).

15.* S. Sivaramakrishnan, H. Bai, B.G. Thomas, P. Vanka, P. Dauby and M. Assar: "Transient Flow Structures in Continuous Cast Steel", in *Ironmaking Conference Proceedings*, vol. 59, ISS, Warrendale, PA, Pittsburgh, PA, 2000, pp. 541-57.

16.* H. Bai and B.G. Thomas: "Two-Phase Flow in Tundish Nozzles During Continuous Casting of Steel", in *Materials Processing in the Computer Age*, vol. 3, V. Voller and H. Henein, eds., TMS, Warrendale, PA, 2000, pp. 85-99.

17.* D. Creech: *Computational Modeling of Multiphase Turbulent Fluid Flow and Heat Transfer in the Continuous Slab Casting Mold*, M.S. Thesis, University of Illinois at Urbana-Champaign, 1998.

18.* B.G. Thomas and H. Bai: "Tundish Nozzle Clogging – Application of Computational Models", in *Process Technol. Conf. Proc.*, vol. 18, Iron and Steel Society, Warrendale, PA, 2001, p. in press.

19.* H. Bai and B.G. Thomas: "Bubble Formation during Horizontal Gas Injection into Downward Flowing Liquid", *Metallurgical and Materials Transactions B,* 2001,, p. under review.

20. L. Zhang and S. Taniguchi: "Water Model Study on Inclusion Removal from Liquid Steel by Bubble Flotation", *ISIJ International,* 2001, vol. in press.

* Please note that the indicated references are available to CCC members (including LTV) at our website bgtibm1.me.uiuc.edu in the download section.

Table IA Parameters for water model for Case A (55 ipm+11% gas)

	Normal Conditions	Enlarged Slide Gate
Mold Width W (mm) x Thickness H (mm)	730 x 80	730 x 80
Mold Height (mm)	950	950
Nozzle Submergence Depth (top surface to top of port)	80	80
Nozzle Inner Diameter *(mm)*	31	31
Nozzle Port Width (mm) x Height (mm)	31 x 31	31 x 31
Jet Angle	30° down	30° down
Inlet Jet Spread Angle	0°	0°
Water Flow Rate Q_w *(SLPM)*	58.59 (15.5 GPM)	76.06 (20.1 GPM)
Equivalent Steel Casting Speed (ipm) $V_c = \frac{Q_w}{0.4 \times W \times 0.4 \times H \times \sqrt{0.4}}$	54.03	70.14
Gas Flow Rate *(SLPM, hot volume)*	7.43 (15.8 SCFH)	7.43 (15.8 SCFH)
Gas Volume Fraction (%)	11.3	8.9
Inlet Velocity, V_x *(m/s)*	0.571	0.724
Inlet Velocity, V_z*(m/s)*	0.330	0.418
Inlet Turbulent Kinetic Energy, K_o (m^2/s^2)	0.044	0.044
Inlet Turbulence Dissipation Rate,ε_o (m^2/s^3)	0.999	0.999
Water Density (kg/m^3)	1000	1000
Water Viscosity (m^2/s)	1×10^{-3}	1×10^{-3}
Gas Density (kg/m^3)	1.20	1.20
Gas Viscosity (m^2/s)	1.7×10^{-5}	1.7×10^{-5}
Average Bubble Diameter *(mm)*	2.590	2.590
Volume Fraction of 0.5 mm Bubble (%)	1.07	1.07
Volume Fraction of 1.5 mm Bubble (%)	4.53	4.53
Volume Fraction of 2.5 mm Bubble (%)	31.15	31.15
Volume Fraction of 3.5 mm Bubble (%)	55.83	55.83
Volume Fraction of 4.5 mm Bubble (%)	7.42	7.42
Breakup Coefficient	0.5	0.5
Coalescence Coefficient	0	0

Table IB Parameter for water model for Case B (35 ipm/8.5% gas)

	Normal Conditions	Enlarged Slide Gate
Mold Width W (mm) x Thickness H (mm)	730 x 80	730 x 80
Mold Height *(mm)*	950	950
Nozzle Submergence Depth	80	80
Nozzle Inner Diameter *(mm)*	31	31
Nozzle Port Width (mm) x Height (mm)	31 x 31	31 x 31
Water Flow Rate *(SLPM)*	37.80 (10.0 GPM)	43.64 (11.54 GPM)
Equivalent Steel Casting Speed (ipm) $V_c = \frac{Q_w}{0.4 \times W \times 0.4 \times H \times \sqrt{0.4}}$	34.86	40.24
Gas Flow Rate *(SLPM, hot volume)*	3.71 (7.9 SCFH)	3.71 (7.9 SCFH)
Gas Volume Fraction (%)	8.9	7.8
Inlet Velocity, V_x *(m/s)*	0.358	0.410
Inlet Velocity, V_z*(m/s)*	0.207	0.237
Inlet Turbulent Kinetic Energy *(m^2/s^2)*	0.044	0.044
Inlet Turbulence Dissipation Rate *(m^2/s^3)*	0.999	0.999
Water Density *(kg/m^3)*	1000	1000
Water Viscosity *(m^2/s)*	1×10^{-3}	1×10^{-3}
Gas Density *(kg/m^3)*	1.20	1.20
Gas Viscosity *(m^2/s)*	1.7×10^{-5}	1.7×10^{-5}
Jet Angle	30° down	30° down
Inlet Jet Spread Angle	0°	0°
Average Bubble Diameter *(mm)*	2.43	2.43
Volume Fraction of 0.5 mm Bubble (%)	4.43	4.43
Volume Fraction of 1.5 mm Bubble (%)	4.90	4.90
Volume Fraction of 2.5 mm Bubble (%)	10.34	10.34
Volume Fraction of 3.5 mm Bubble (%)	8.73	8.73
Volume Fraction of 4.5 mm Bubble (%)	11.60	11.60
Volume Fraction of 5.5 mm Bubble (%)	12.71	12.71
Volume Fraction of 6.5 mm Bubble (%)	0	0
Volume Fraction of 7.5 mm Bubble (%)	0	0
Volume Fraction of 8.5 mm Bubble (%)	0	0
Volume Fraction of 9.5 mm Bubble (%)	21.83	21.83
Volume Fraction of 10.5 mm Bubble (%)	25.46	25.46
Breakup Coefficient	0.1	0.1
Coalescence Coefficient	0	0

Table II Parameters in the real caster modeling

	Case A (13 SLPM, 55 ipm)	Case B (6.3SLPM /13SLPM, 35 ipm)
Mold Width	1854 *mm*	
Mold Thickness	228 *mm*	
Nozzle Submergence Depth (top surface to top of port)	165 *mm*	
Nozzle Bore Inner Diameter	78 *mm*	
Nozzle Port Height	78 *mm*	
Nozzle Port Width	78*mm*	
Vertical Velocity in Nozzle	2.05 *m/s*	1.31 *m/s*
Nominal Vertical Angle of Port Edges	15° down	
Inlet Jet Spread Angle	0°	
Casting Speed, V_c	23.2 *mm/s*	14.8 *mm/s*
Liquid Steel Density, ρ_l	7020 kg/m^3	
Gas Density, ρ_{gas}	0.27 kg/m^3	
Steel Laminar (Molecular) Viscosity, μ_o	0.00560 *kg/m s*	
Gas Vescosity, μ_{gas}	7.42E-5	
Surface Tension Coeff. (Steel-Argon)	1.192 *N/m*	
Inlet steel flow rate	0.584 m^3/min	0.376 m^3/min
Throughput (ton/min)	4.10	2.64
Inlet Gas Flow Rate	13 *SLPM*	6.3*SLPM* /13 *SLPM*
Inlet Gas Volume Fraction, f_{gas}	11%	8.5%
Average Gas Bubble Diameter, D_o	2.59 *mm*	2.43 mm
Gravitational Acceleration, g	9.8 m/s^2	

*Blank in second column is the same as the first column.

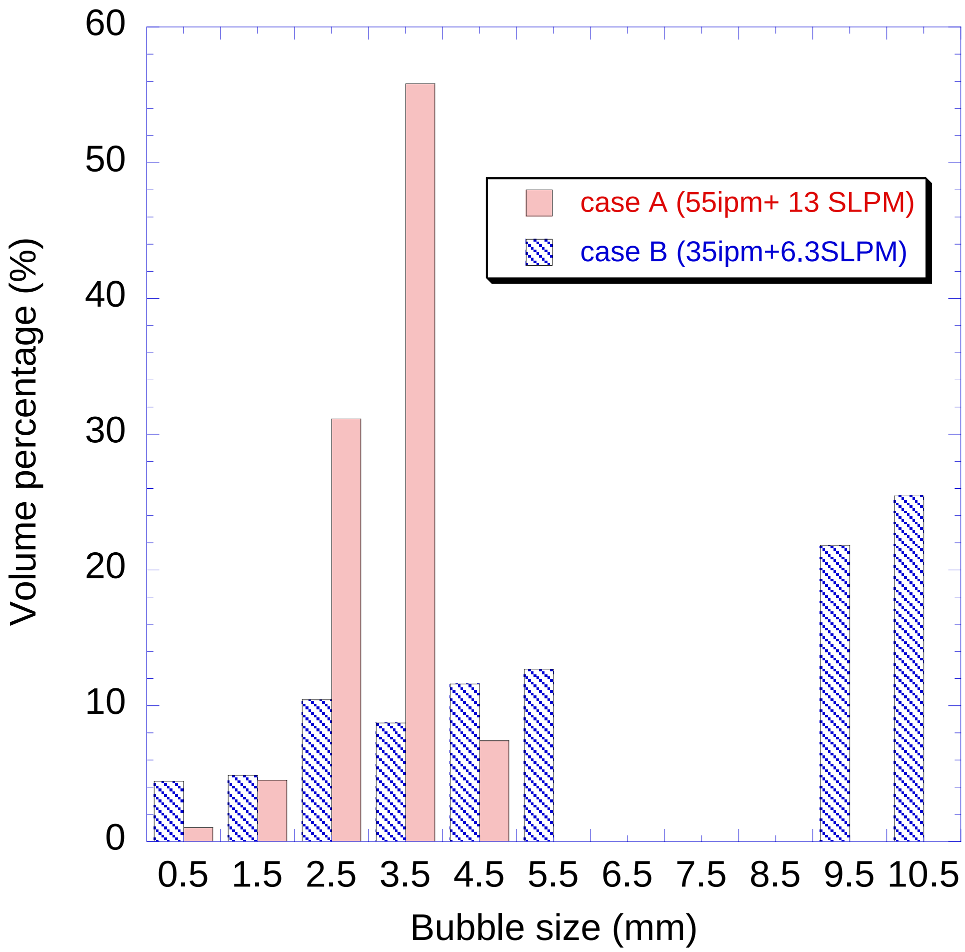

Fig. 1 Bubble size distribution in the mold (measurements in 0.4 scaled water model)

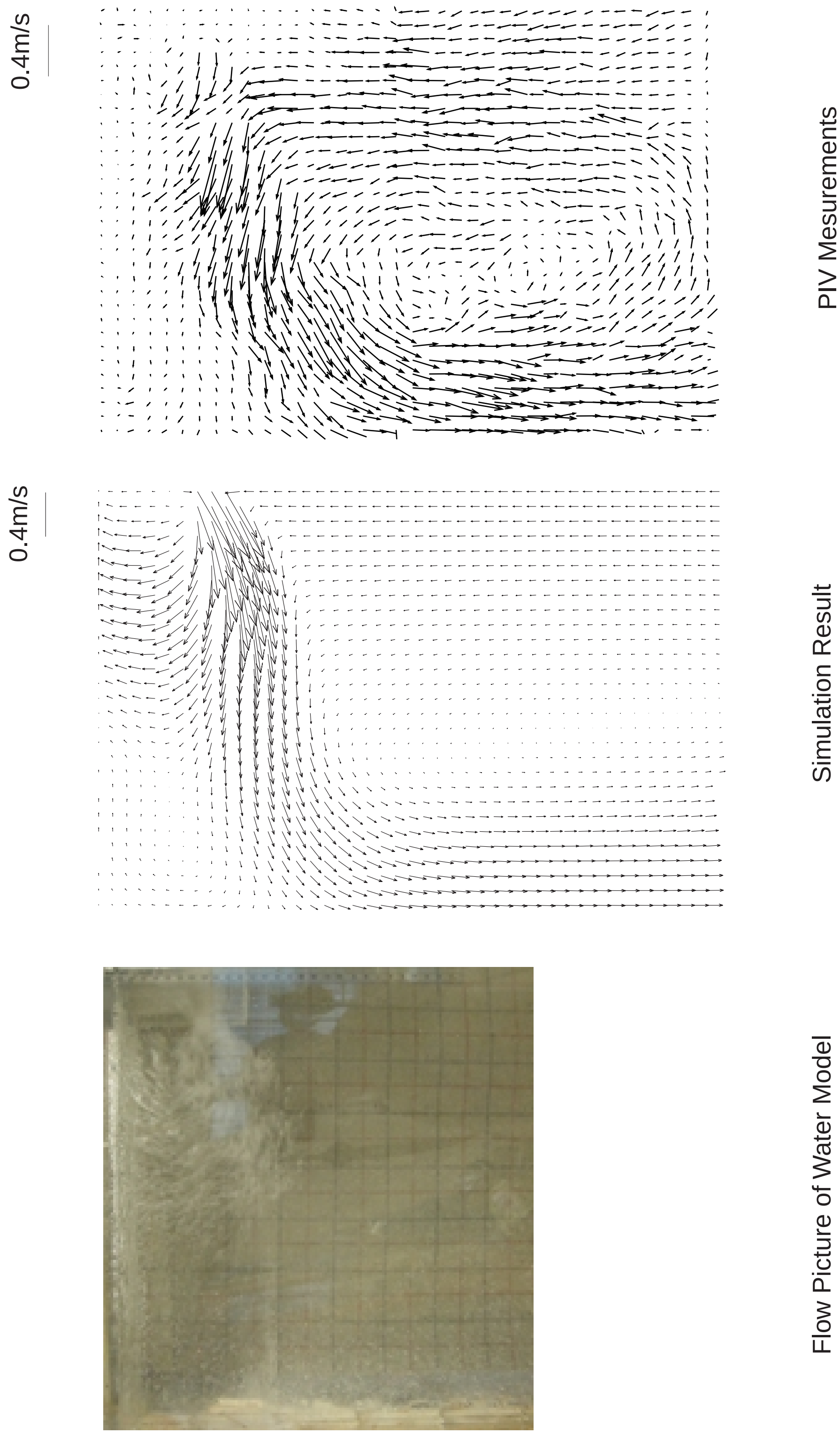

Fig. 2A Comparison of velocity at centerplane between PIV measurements, Simulation and eyeview

(55 ipm + 13 SLPM/11% hot gas)

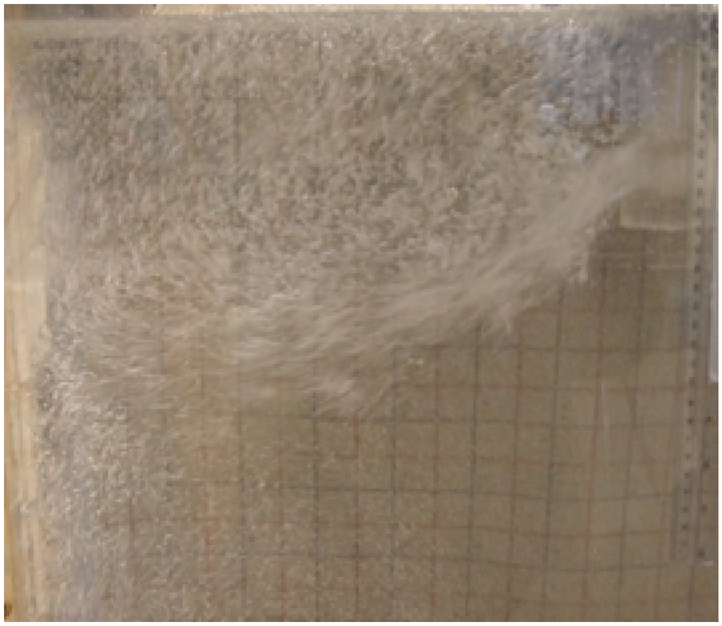

Flow Picture of Water Model (55ipm +11% gas)

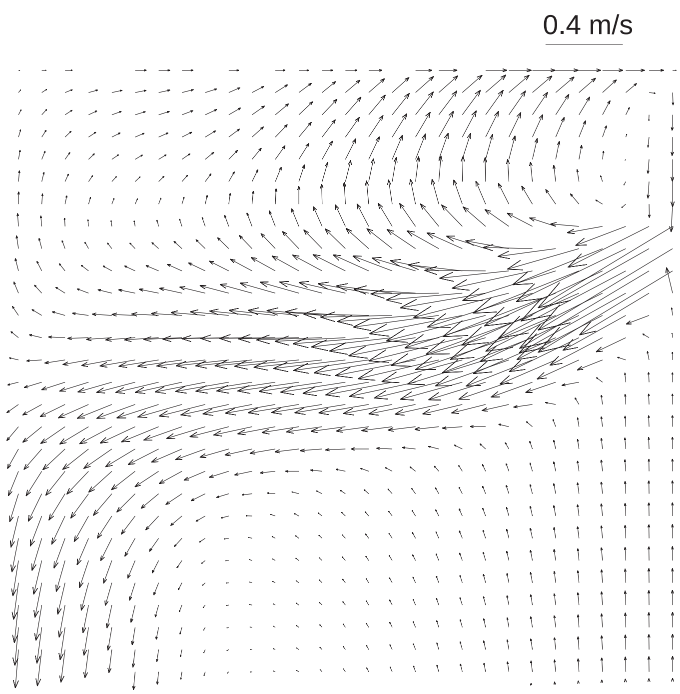

Liquid Velocity Vectors of Modeling (55ipm+11%gas)

Fig. 3A Comparison of simulation and eyeviews
while adjusting liquid level with 15% increase in flow rate
(55 ipm + 13 SLPM/11% hot gas)

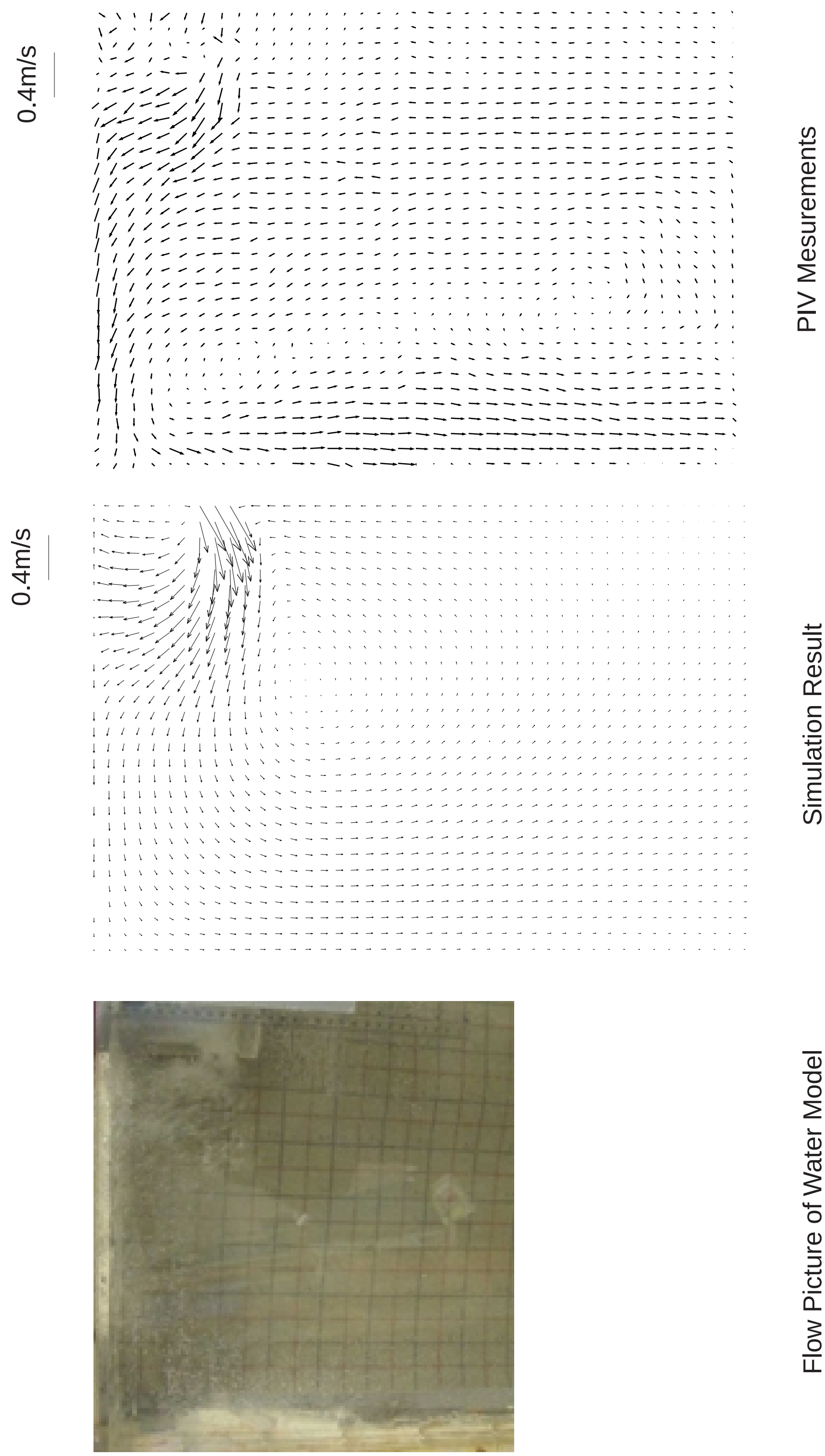

Fig. 2B Comparison of velocity at centerplan between PIV measurements, Simulation and eyeview
(35 ipm + 6.3 SLPM/8.5% hot gas)

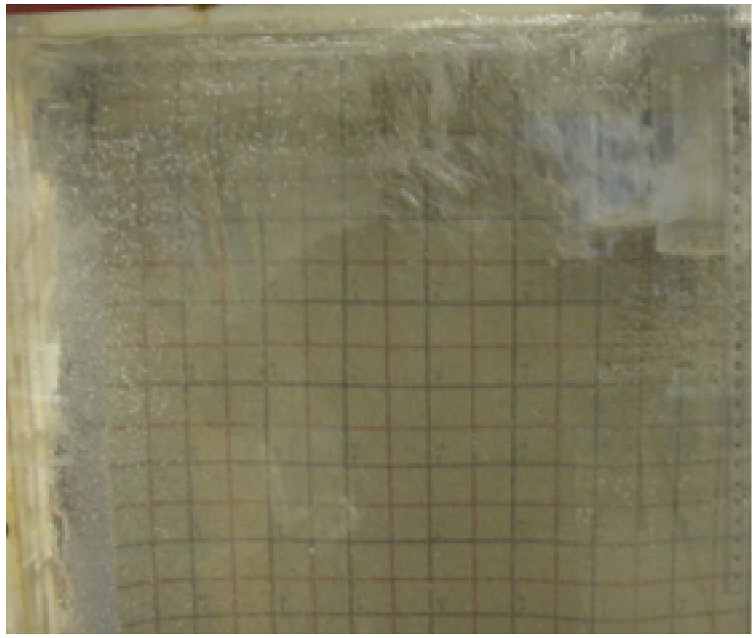

Flow Picture of Water Model (35ipm +8.5% gas)

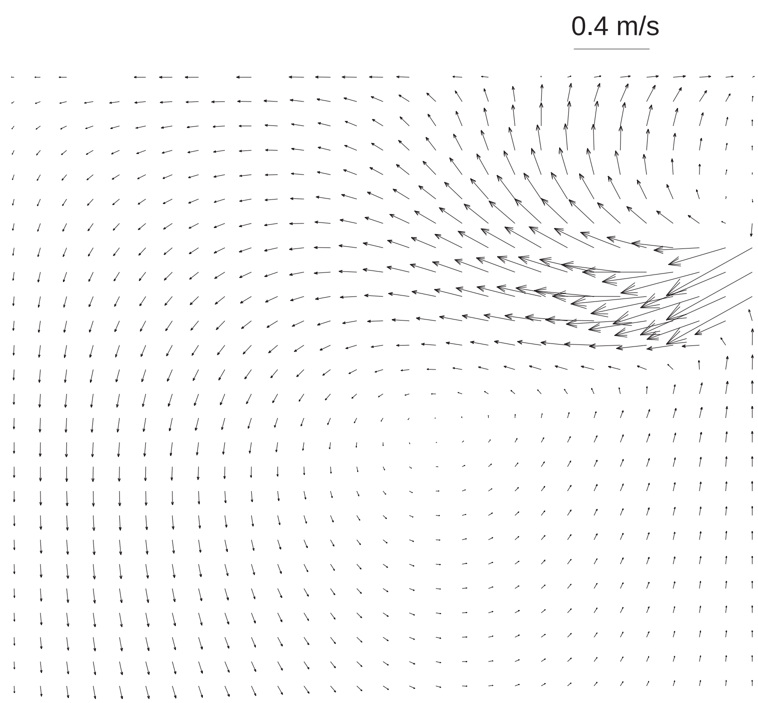

Liquid Velocity Vectors of Modeling (35ipm+8.5%gas)

Fig. 3B Comparison of simulation and eyeviews
while adjusting liquid level with 15% increase in flow rate
(35 ipm + 6.3 SLPM/8.5% hot gas)

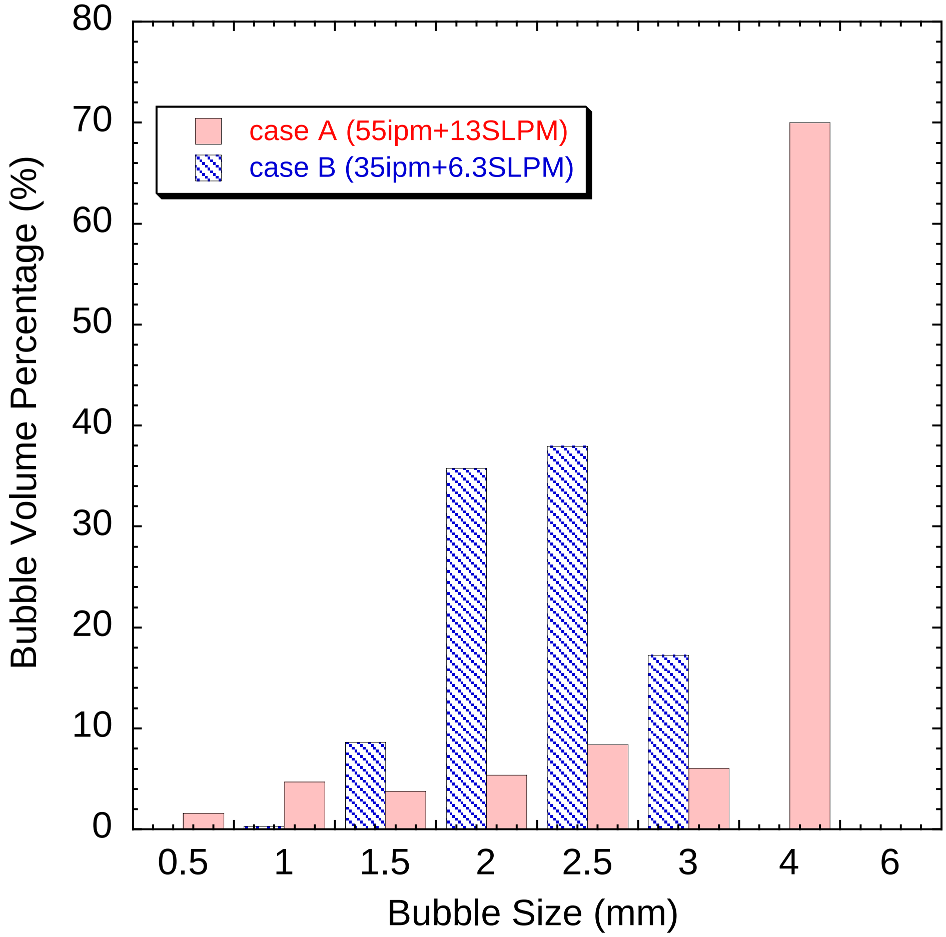

Fig. 4 Assumed bubble size distribution in the steel caster nozzle (based on double-needle experimental measurements)

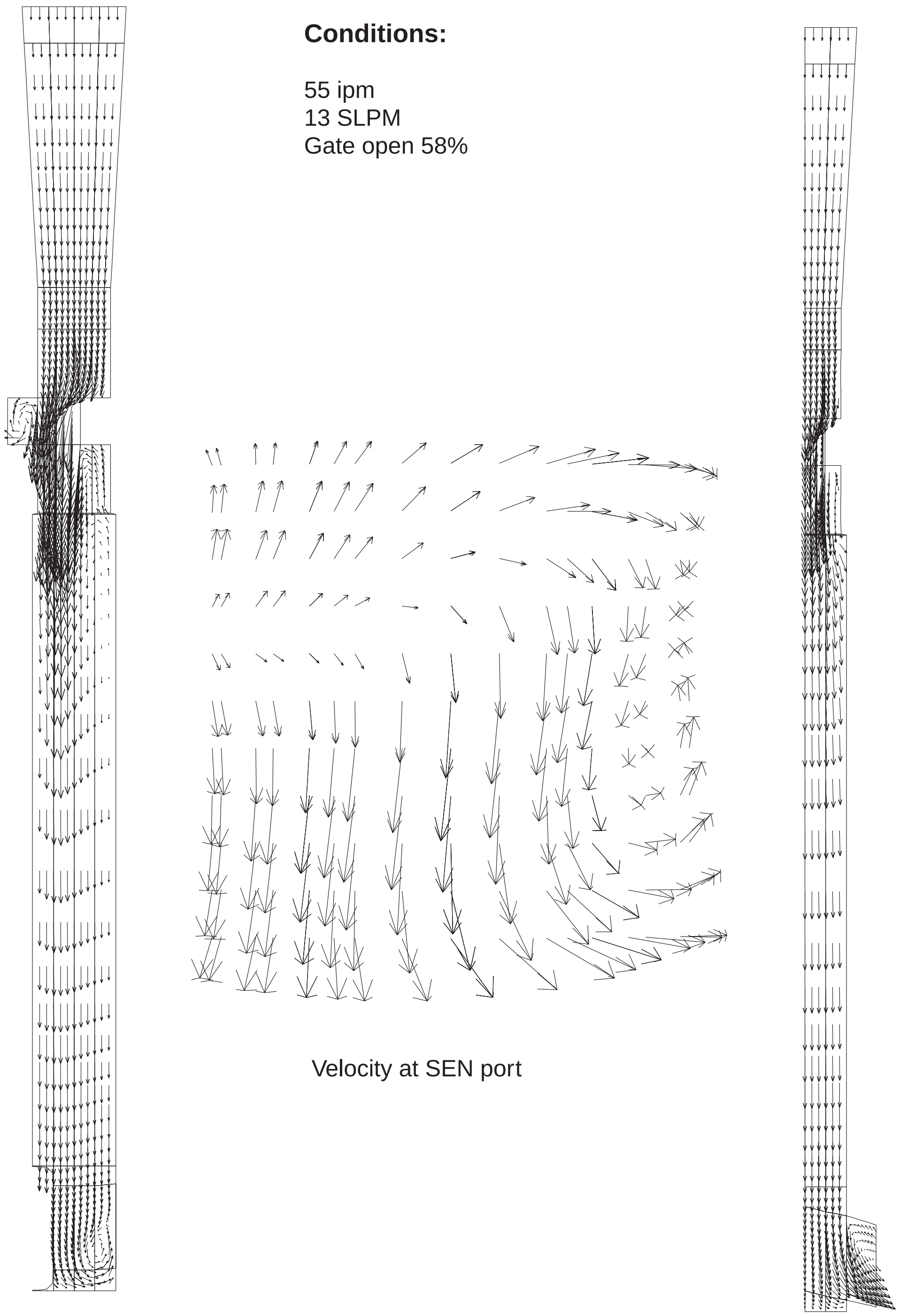

Centerplane parallel to SEN port

Centerplane perpendicular to SEN port

Fig. 5A Liquid velocity in the nozzle

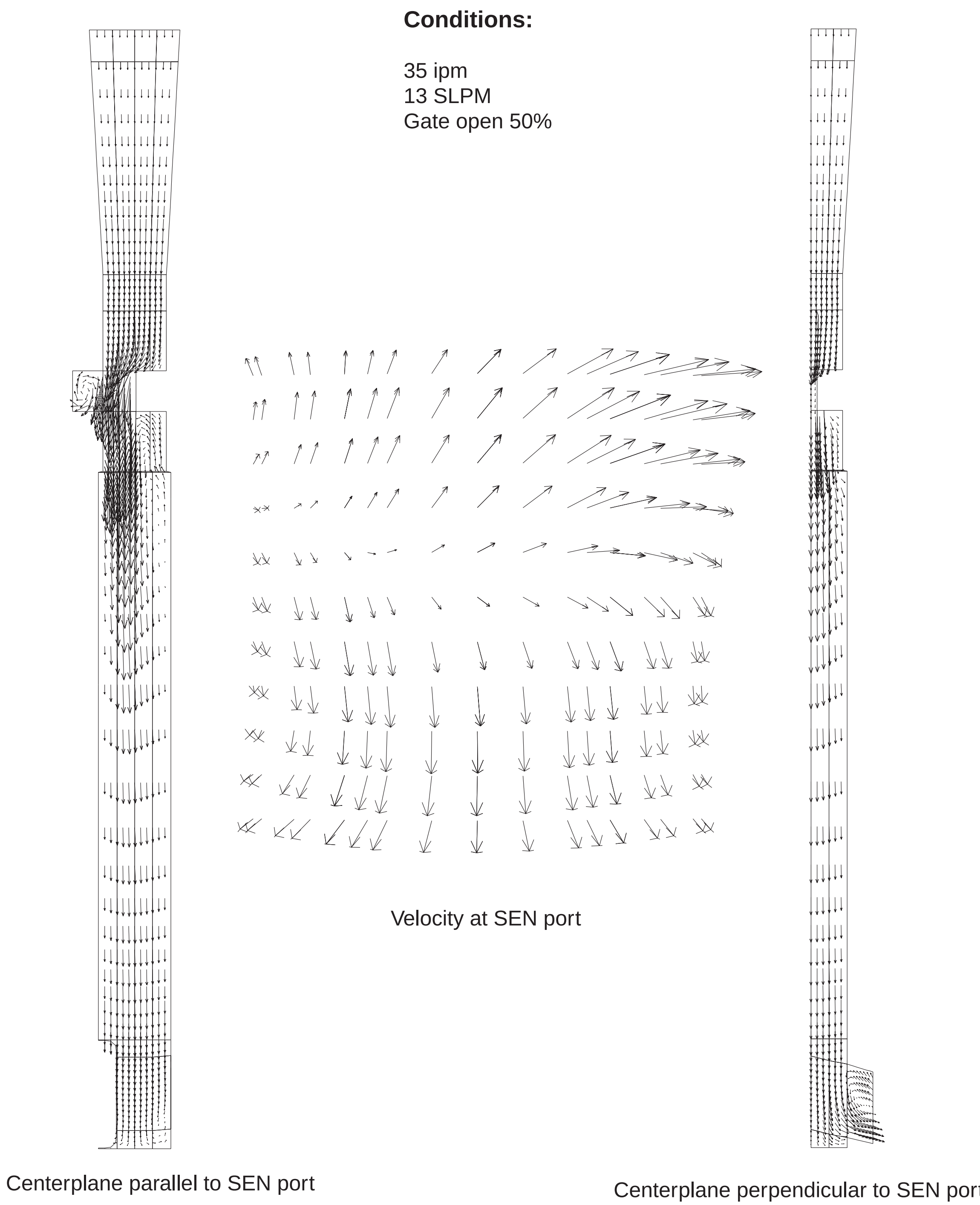

Fig. 5B Liquid velocity in the nozzle

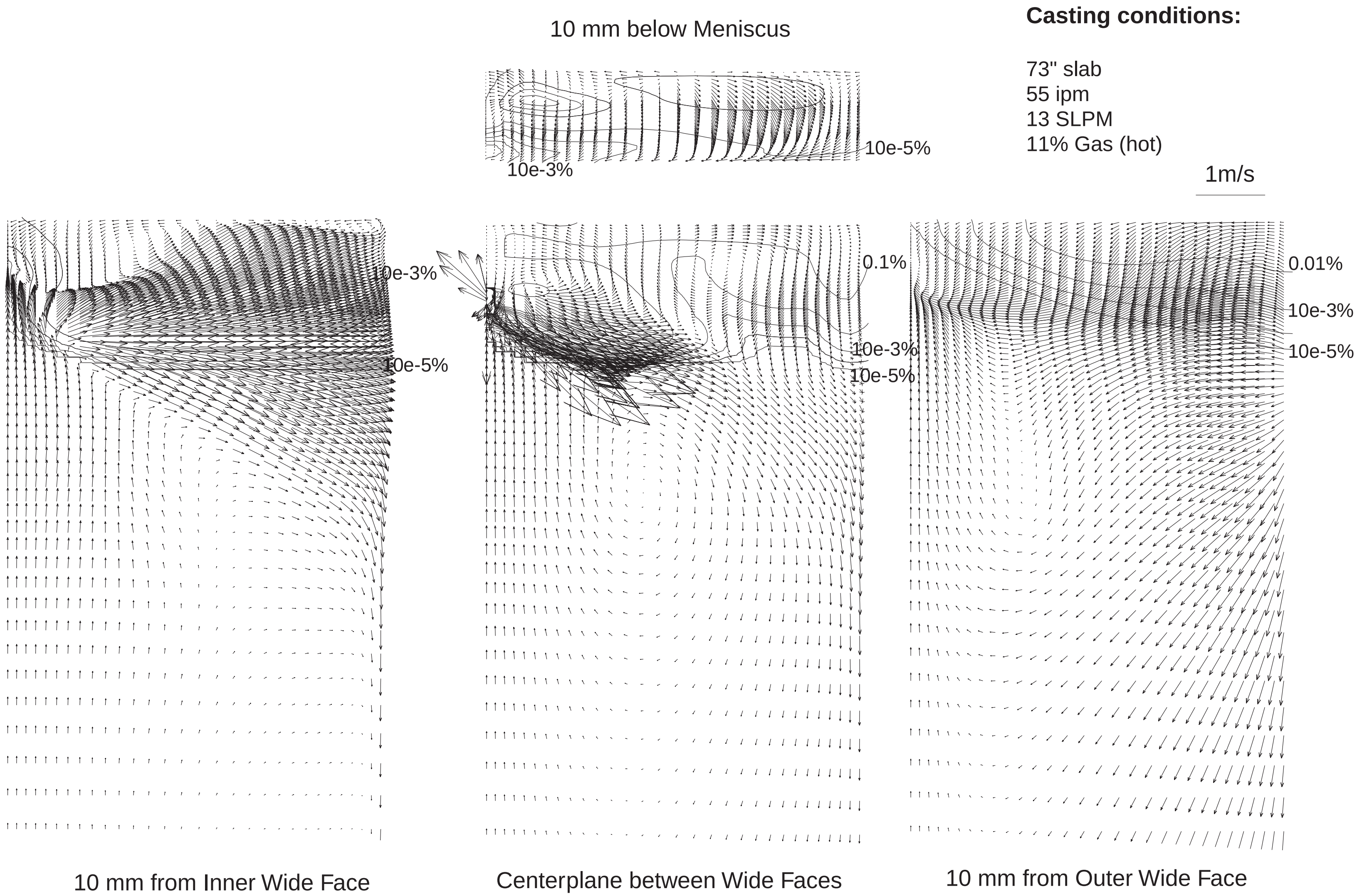

Fig. 6A Steel flow pattern calculated using CFX with distributed bubble size (2.59mm mean)

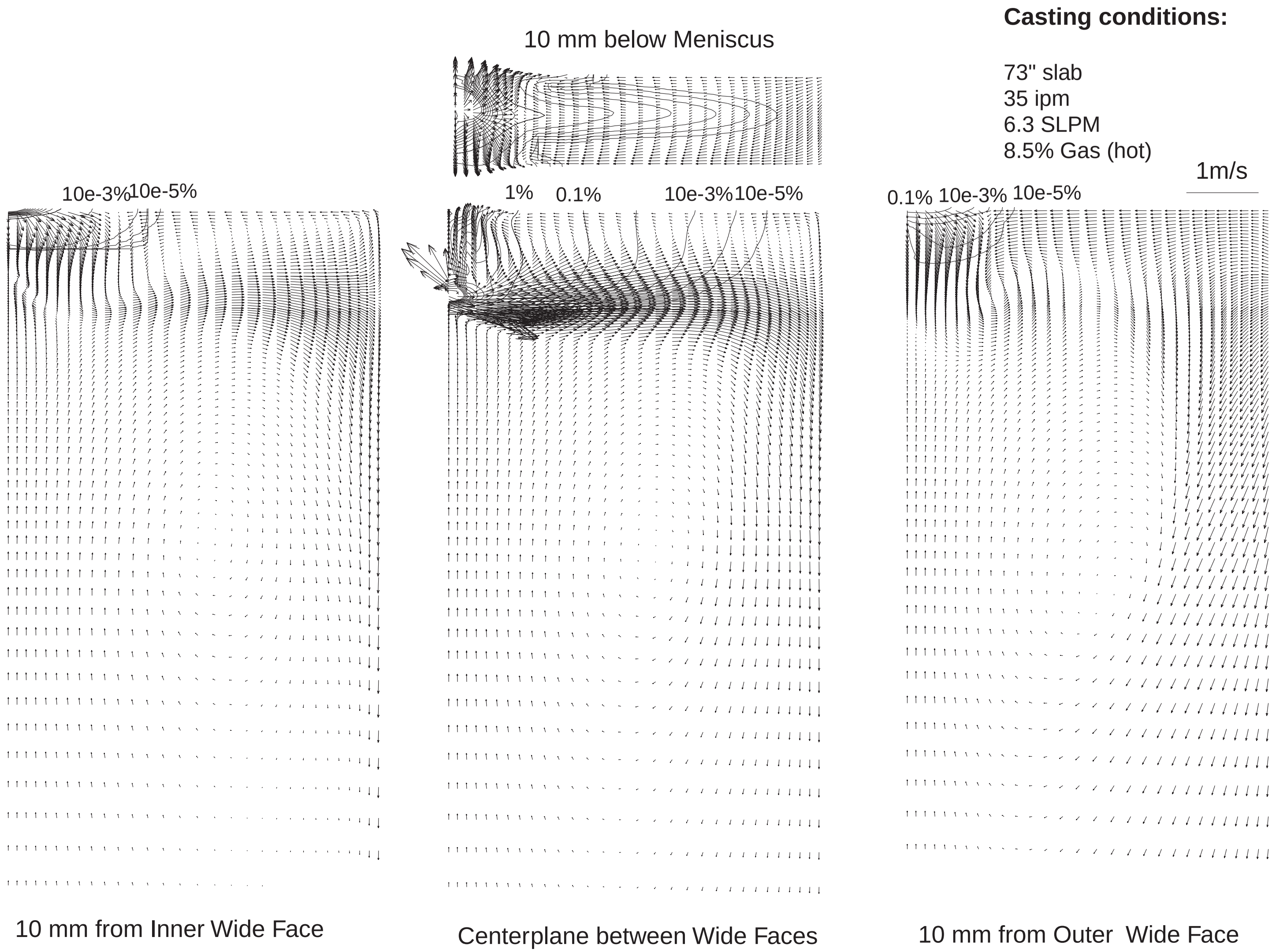

Fig. 6B Steel flow pattern calculated using CFX with distributed bubble size(2.43 mm mean)

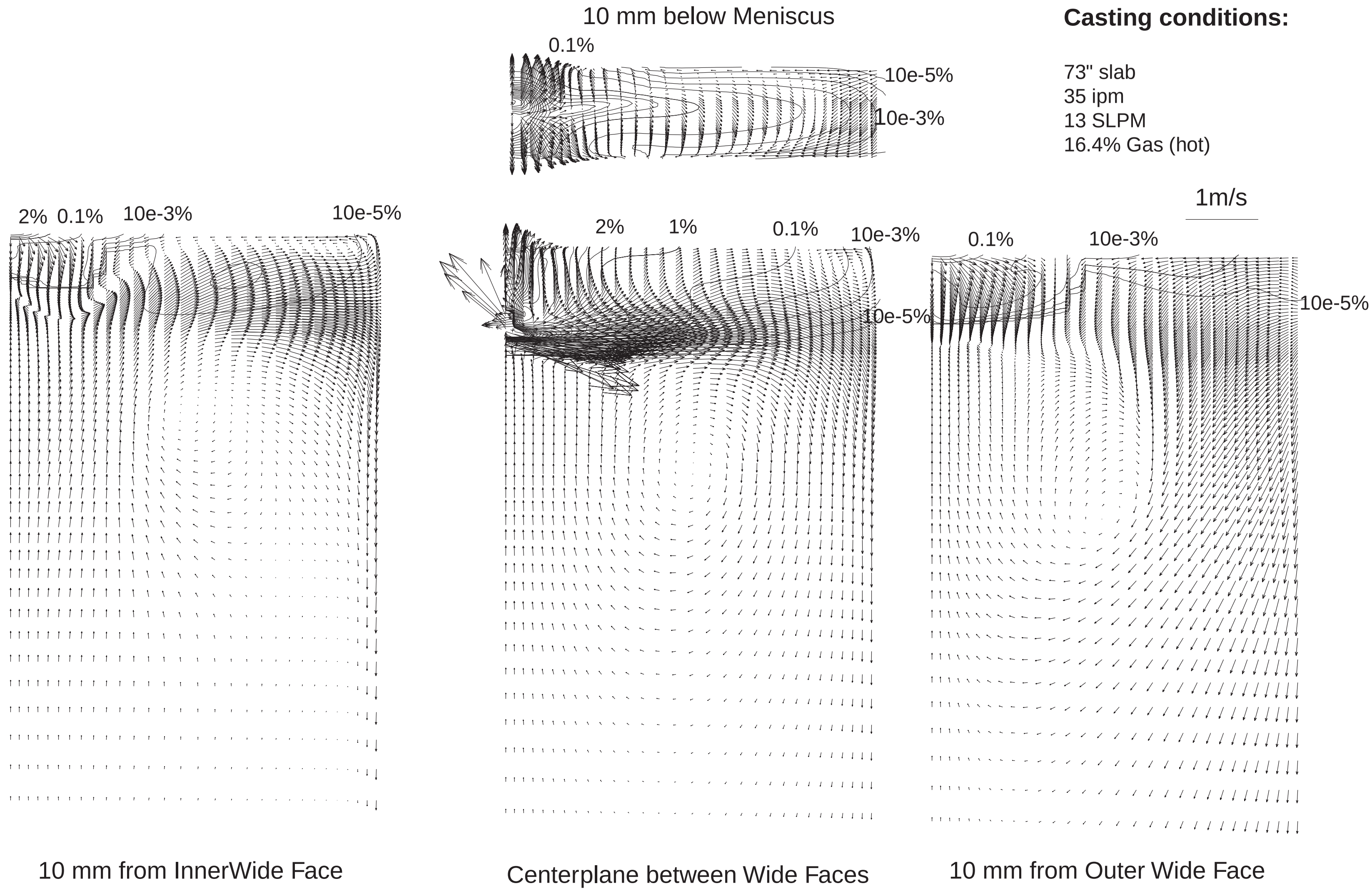

Fig. 6C Steel Flow pattern calculated using CFX with distributed bubble size(2.43 mm mean)

Conditions: 73" slab, 55ipm, 13 SLPM, 11% Gas (hot))

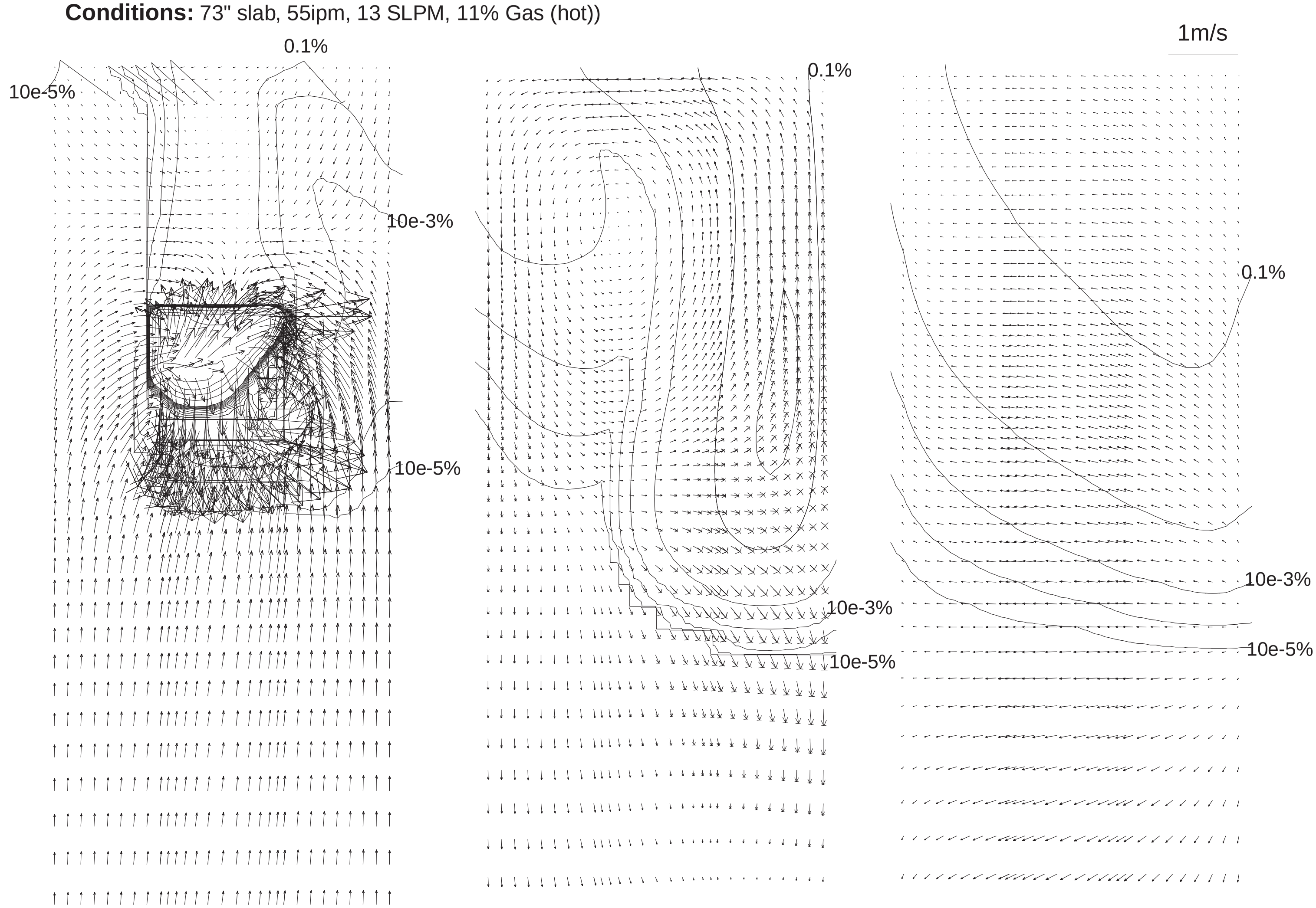

Fig. 7A Steel flow pattern calculated using CFX with distributed bobble size(2.59 mm mean)

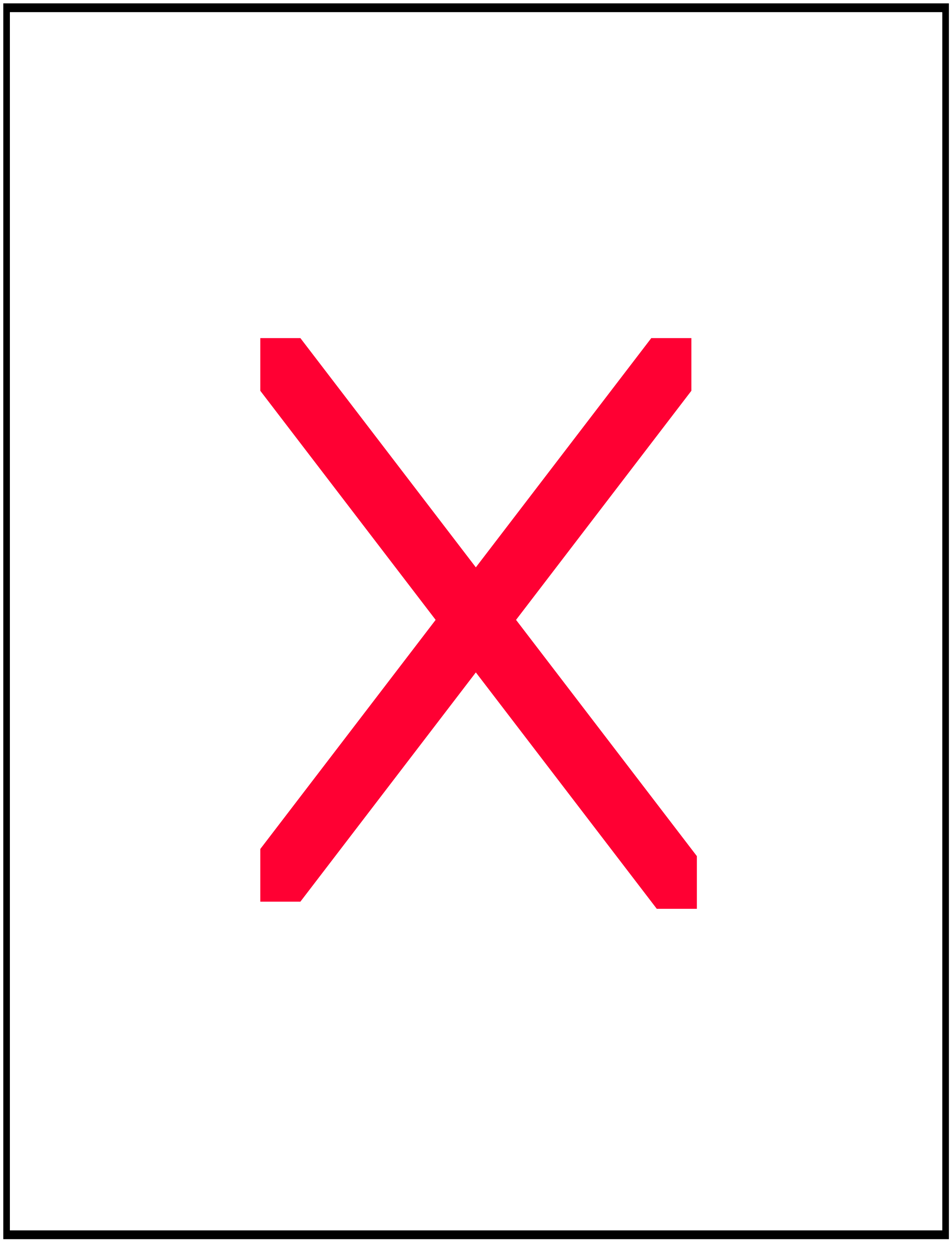

Conditions: 73" slab, 35ipm, 13 SLPM, 16.4% Gas (hot))

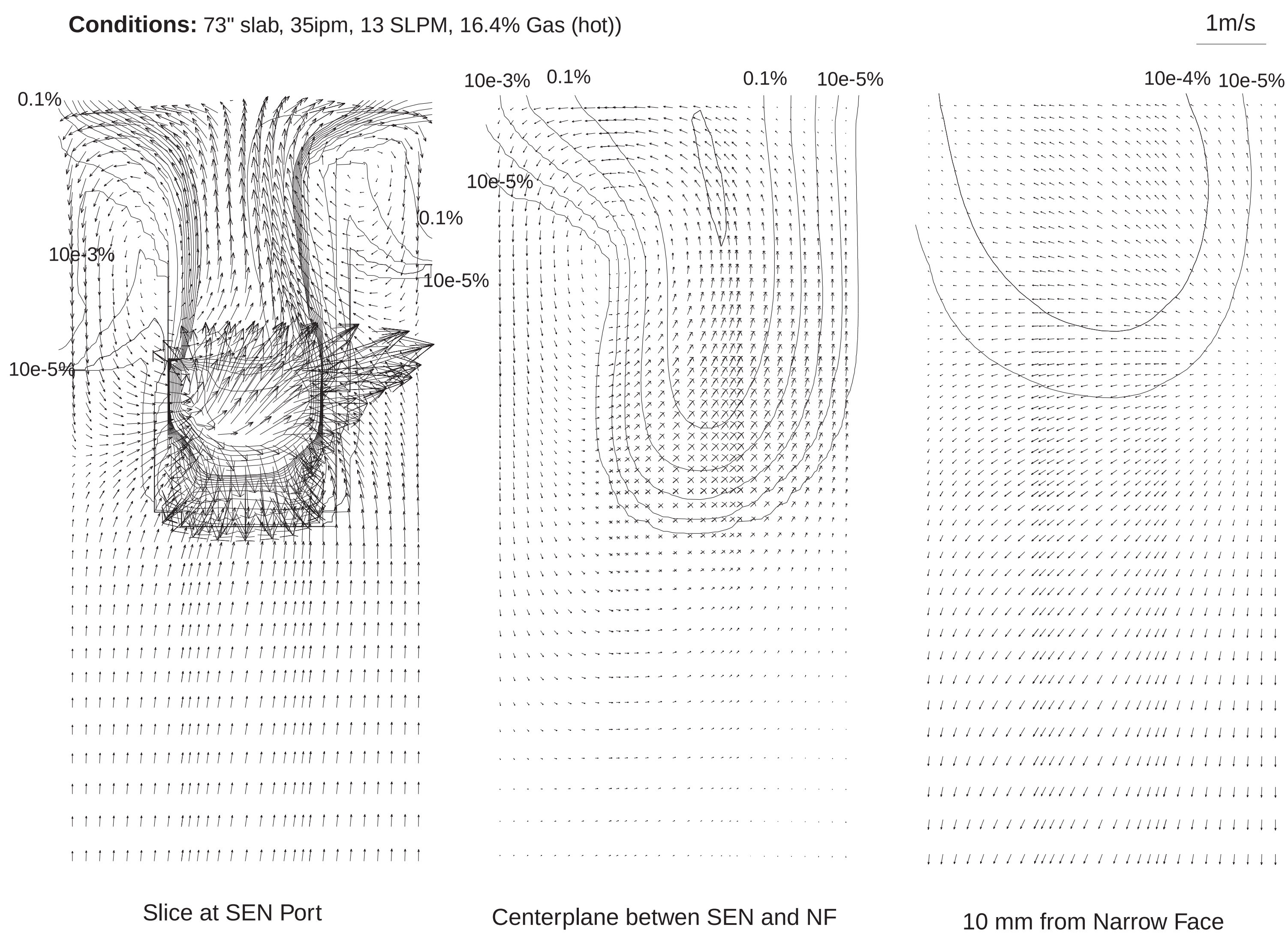

Fi.g 7C Steel flow pattern calculated using CFX with distributed bobble size(2.43 mm mean)

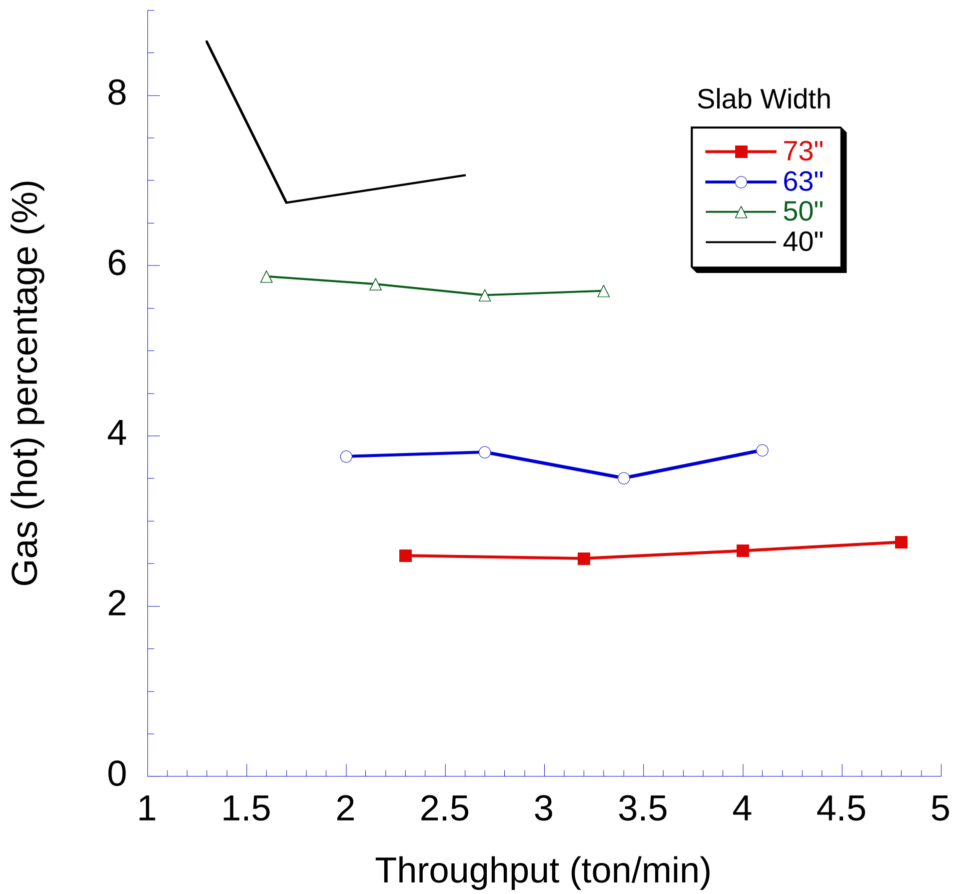

Fig. 8 Flow pattern Identification (Water model)

**modified from M. Assar, P. Dauby and G. Lawson,
2000 steelmaking conf. proceedings, p403.

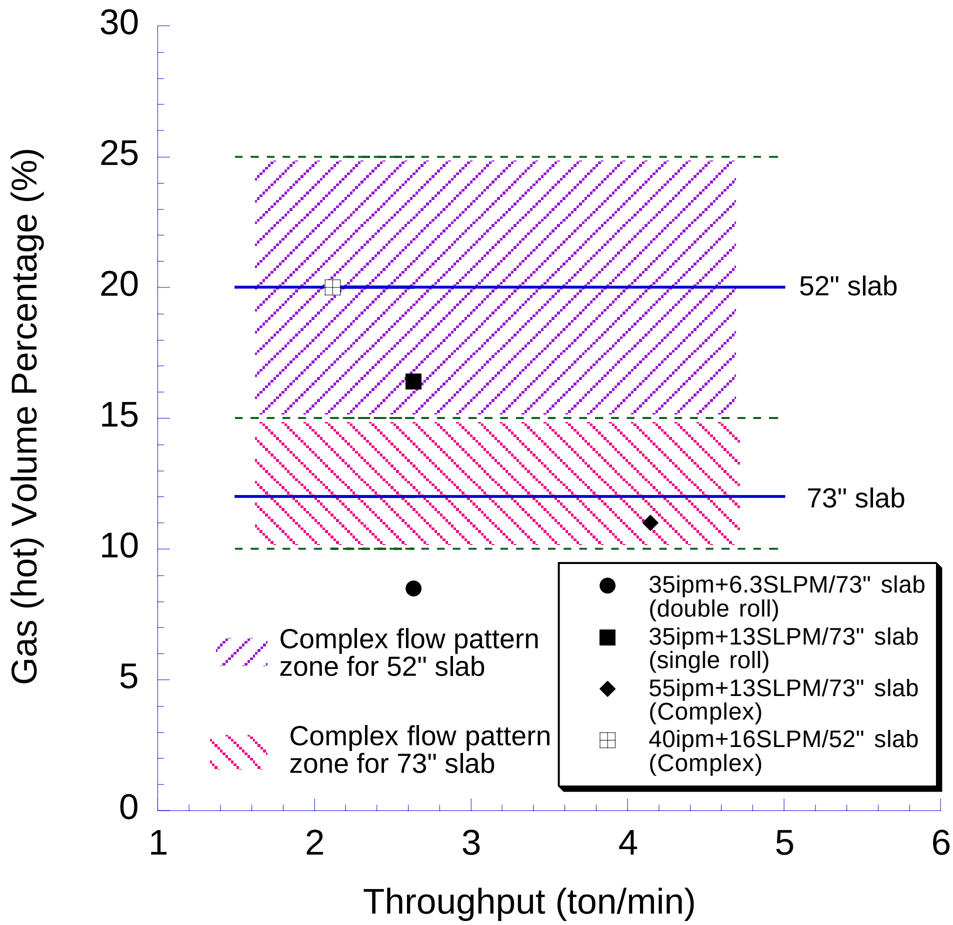

Fig. 9 Flow pattern identification in steel caster (from simulation of real caster)

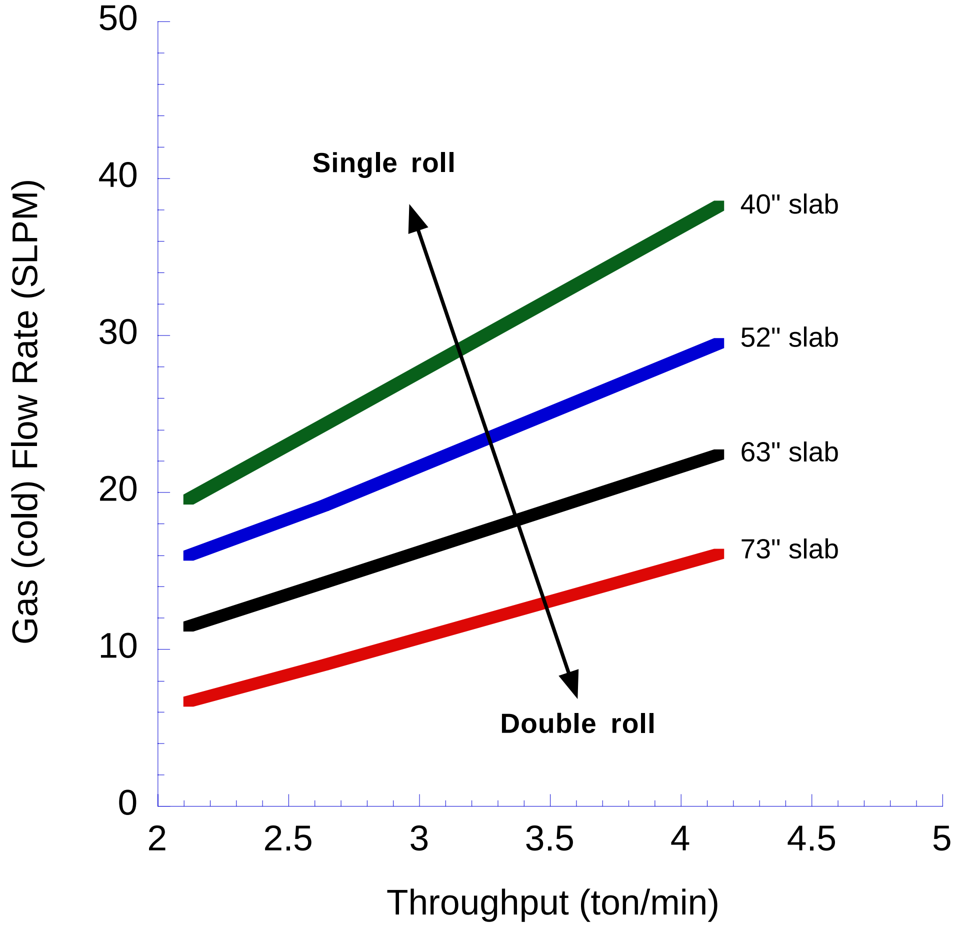

Fig. 10 Flow pattern identification (from simulation of real caster)

Appendix I Investigation of Bubble Size Distributions

Gas bubble size has an important effect on the flow pattern. The bubble size that forms when gas is injected into flowing liquid depends mainly on the vertical liquid velocity, the gas flow rates per orifice and the contact angle.[19] In order to perform accurate simulations, actual size distributions were measured in the water model at two different conditions (cases A and B in Table I). In addition, bubble sizes were estimated in the steel caster, based on the model of Bai for the corresponding flow conditions in the steel casting nozzle.[19]

The bubble size in the water model was measured for two cases (A and B in Table I) by measuring the diameters of individual bubbles in instantaneous photographs of the water model. Two such photographs are shown in Figs. A.IA and A.IB. The results are tabulated in Table A.I.

The bubble size in the steel caster was estimated based on the model of Bai.[19] First, the number of active of sites on the refractory surface is estimated to be about 200, based on a total inner surface area of porous refractory of 12246 mm^2 (78mm bore x 50 mm high) and assuming 60 mm^2 of surface area per active site from recent experiments.[20] For the high vertical velocity in the nozzle for these conditions, Bai's bubble formation model[19] suggests that the mean bubble size increase in the steel argon system should be small, relative to that in the water model. Thus, the distribution assumed in the present simulations was taken directly from measurements from Bai's video images of flow in the water model for these two cases (A and B in Table I). The measured results are tabulated in Table A.II.

The bubble size in the scale water model at LTV Steel is different from that in the steel caster for several reasons. Firstly, single large slit injecting the gas into the water model produces generally larger bubbles, relative to those from the many active sites in the refractory walls. The large, but narrow slit also encourages nonuniform bubble sizes. Secondly, the difference in fluid properties (argon bubbles in steel are slightly larger than air bubbles in water for the same flow rate, owing to the higher surface tension and contact angle). Thirdly, the slower liquid flow rate in the small (0.4-scale) water model allows significant bubble growth prior to detachment, resulting a non-uniform distribution with a few very large bubbles for case B. When speed is increased (case A), the generally slow gas flow rates produce a more uniform bubble distribution. In the caster, on the other hand, it is expected that the size distribution scatter will have the reversed trend. Bubble size for case B is expected to be relatively uniform, (see Appendix I)), as the liquid flow rate is expected to be above the critical. Increasing gas flow rate in the caster should cause increased scatter in the size distribution, (case A).

Table A.IA Measures bubble size distribution in LTV 0.4-scale water model for Case A (55ipm + 13 SLPM/11% hot gas)

Region	≤1mm	1-2mm	2-3mm	3-4mm	4-5mm	≥5mm
A	>10	16	20	17	2	0
B	>5	8	16	10		
C	>10	9	13	5		
Total	25	33	49	32	2	
Volume (ml)	13.08	58.29	400.68	718.01	95.38	
Volume percentage	1.02%	4.53%	31.15%	55.83%	7.42%	
Average	2.59mm					

Table A.IB Measures bubble size distribution in LTV 0.4-scale water model for Case B (35ipm + 6.3 SLPM/8.5% hot gas)

Region	≤1mm	1-2mm	2-3mm	3-4mm	4-5mm	5-6mm	6-7mm	7-8mm	8-9mm	9-10mm	≥10mm
11	5	2	1								
12	>11	3	1	1							
13	>14	6	4	2	1						
14	>16	4	2	1	1						1
21	9	3									
22	>13	4	1		1						
23	>20	3	2	1							
24	>20	4	2	2		2				1	
31	>10	4									
32	>10	3	2								
33	>17	4	3	1		1					
34	5	6	2		1						
35	6	1	3		1						
44	6	4	1								
45	>12	5	2								
Total	>174	57	26	8	5	3				1	1
Volume (ml)	91.05	100.68	212.60	179.50	238.44	261.20				448.69	523.69
Volume percent	4.43%	4.90%	10.34 %	8.73%	11.60 %	12.71 %				21.83%	25.48%
Average size	2.43mm										

Table A.IIB Measured bubble size distribution for Case Bubble A (55ipm + 13 SLPM/11% hot gas, Q_{air}=1.2ml/s per pore, U_{water}=1.92 m/s) in double-needle experiments

Diameter of bubbles(mm)	<1.0	1.0	1.5	2.0	2.5	3.0	3.0-5.0	>5.0	Photo Frame No.
Data Set #1	4	3	1	1	0	1	1	0	159
Data Set #2	2	0	0	0	0	0	1	0	219
Data Set #3	0	0	0	1	1	0	1	0	265
Data Set #4	2	1	1	0	1	0	1	0	285
Data Set #5	2	2	1	0	1	0	0	0	315
Data Set #6	3	2	0	0	0	1	2	0	368
Data Set #7	0	1	1	0	0	0	2	0	397
Data Set #8	3	2	0	1	0	0	1	0	532
Data Set #9	2	1	1	0	1	0	2	0	631
Data Set #10	1	2	0	1	0	0	2	0	668
Total Number	19	14	5	4	4	2	13	0	
Total Volume (mm^3)	3.73	11.00	8.84	12.57	19.63	14.14	163.3	0	
Volume %	1.6	4.72	3.79	5.39	8.42	6.06	70	0	

Table A.IIB Measured bubble size distribution for Case B (35ipm + 6.3 SLPM/8.5% hot gas, Q_{gas}=1.3ml/s per pore, U_{water}=1.3m/s) in double-needle experiments

Diameter of bubbles(mm)	<1.0	1.0	1.5	2.0	2.5	3.0	>3.0	Photo Frame No.
Data Set #1	0	0	2	5	4	2	0	141
Data Set #2	0	0	3	4	2	3	0	177
Data Set #3	0	0	1	7	3	0	0	211
Data Set #4	0	0	2	7	3	1	0	246
Data Set #5	0	1	6	4	4	0	0	286
Data Set #6	0	0	2	3	6	2	0	341
Data Set #7	0	1	3	7	3	0	0	380
Data Set #8	0	0	2	8	4	2	0	444
Data Set #9	0	0	1	6	5	0	0	481
Data Set #10	0	0	2	5	4	2	0	522
Total Number	0	2	24	56	38	12	0	
Total Volume (mm^3)	0	2.09	56.55	234.57	248.71	113.1	0	
Volume %	0	0.32	8.63	35.81	37.97	17.27	0	

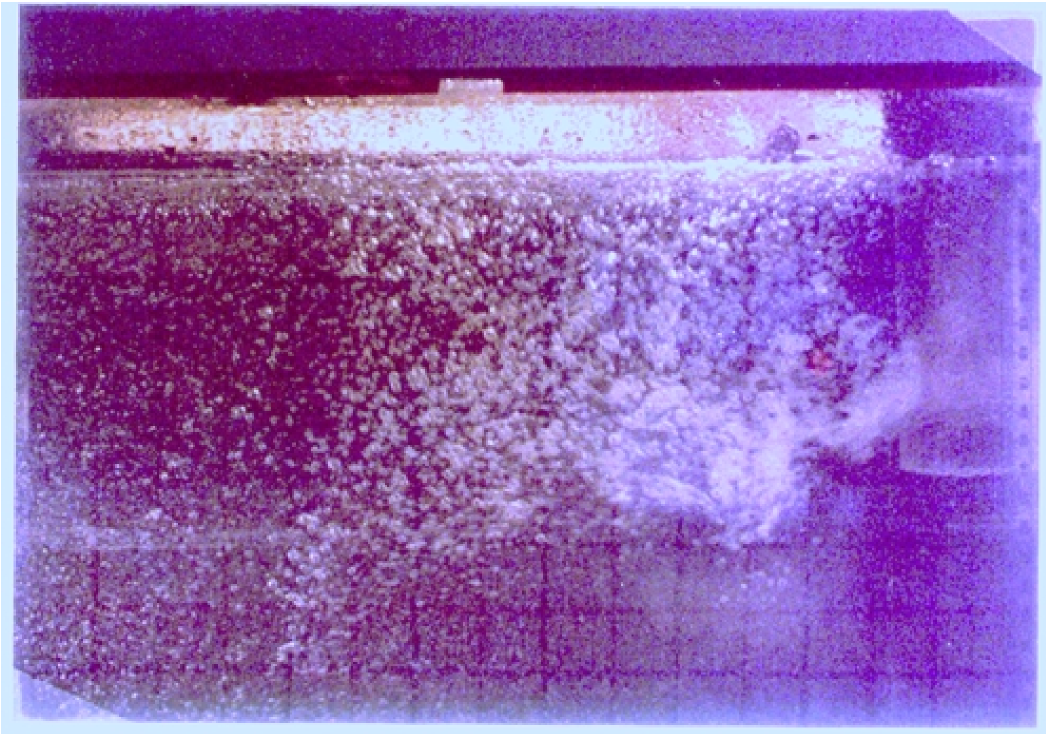

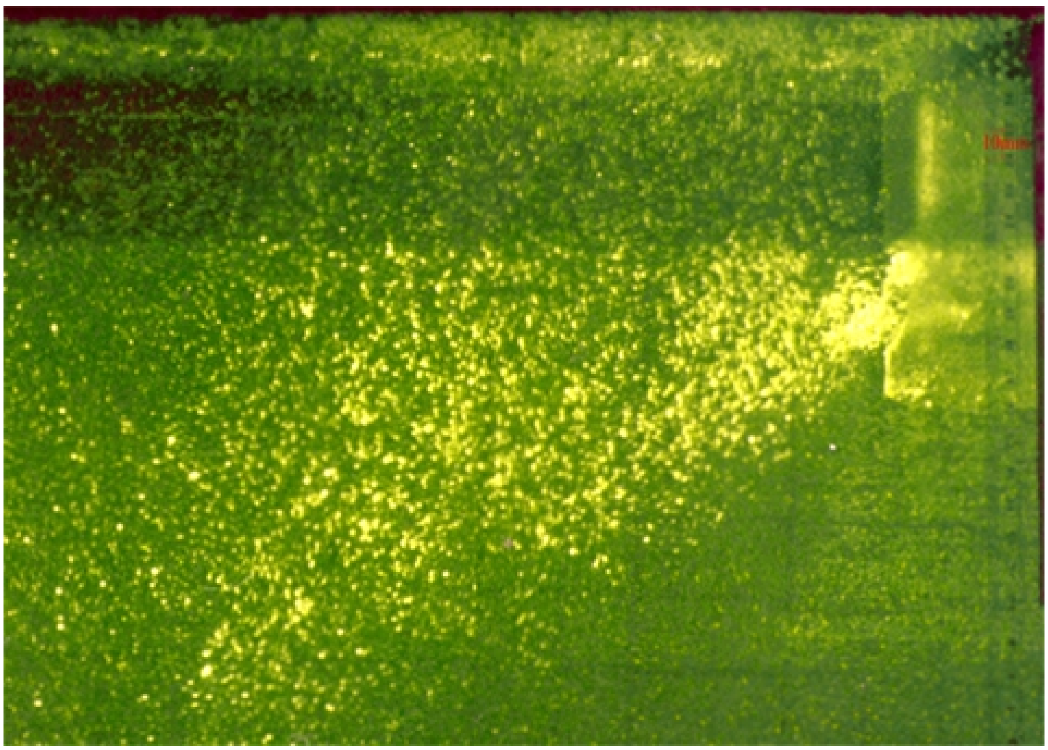

**Fig. A.IA Bubble size in the water model
(55ipm + 13 SLPM/ 11% hot gas)**

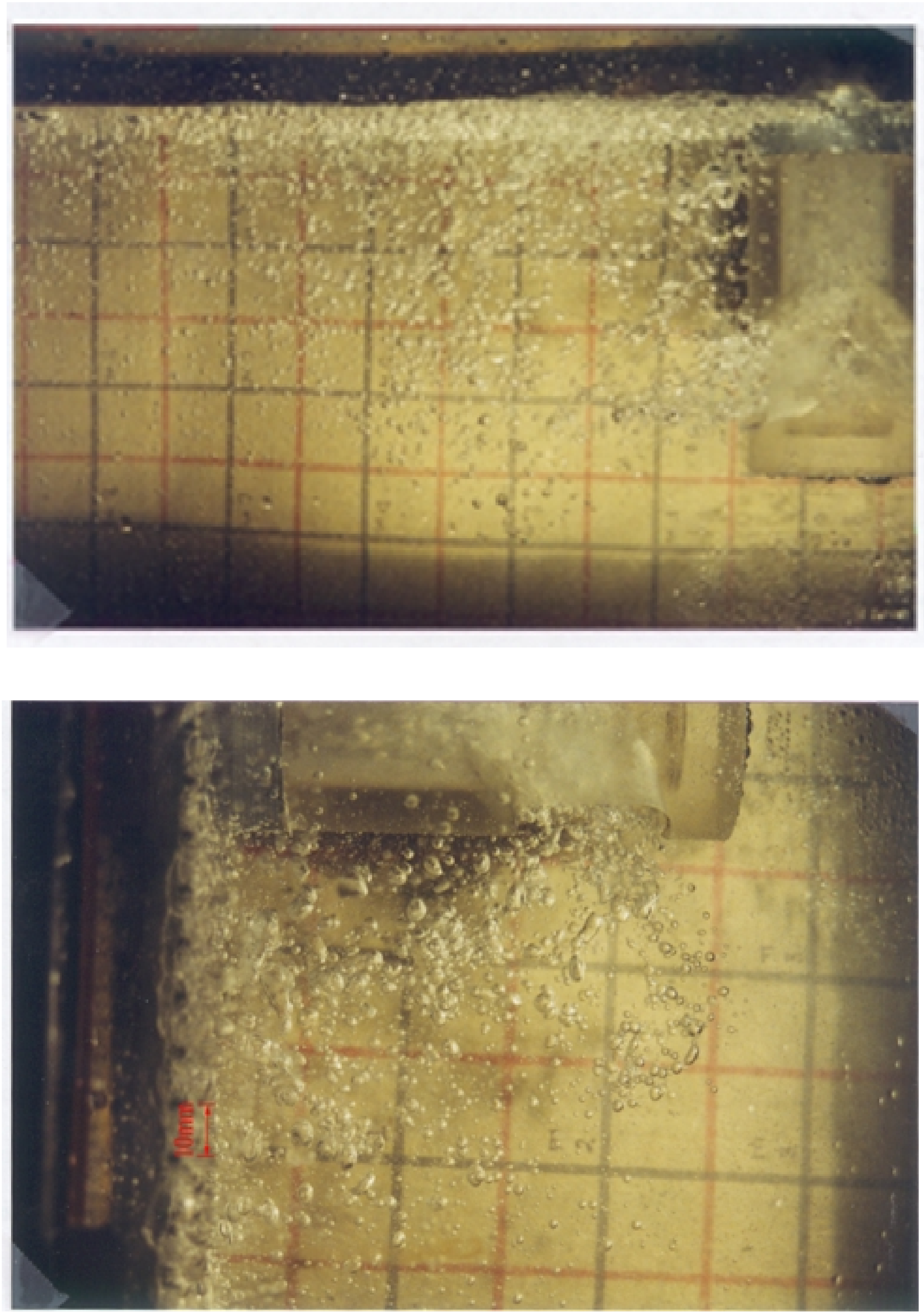

Fig. A.IB Bubble size in the water model
(35ipm + 6.3 SLPM/ 8.5% hot gas)

Appendix II Conversion from hot to cold gas flow rates

Steel flow rate $Q_{liq}(m^3/min)$ = Throughput (ton/min)/7.02(ton/m^3)

The "hot" gas percentage, which is the gas fraction entering the mold cavity in either the steel caster or the water model, can be calculated by:

$$f_{gas} = \frac{Q_{gas}\beta}{Q_{liq} + Q_{gas}\beta}$$

where Q_{gas} is the flow rate of cold gas. The expansion factor β is defined as:

$$\beta = \frac{T_0 P_\infty}{T_\infty (P_\infty + \rho g L_n)}$$

This result turns out to be about 5 times larger than the cold gas percentage. In this calculation, the hot gas percentage is calculated by cold gas percentage multiply 5. The cold gas percentage is calculated by:

$$f_{cold-gas} = \frac{Q_{gas}}{Q_{gas} + Q_{liq}}$$